

## Article

# Solid-Phase Extraction of Organic Dyes on Mixed-Ligand Zr(IV) Metal–Organic Framework

Boris Kharisov <sup>1</sup>, Oxana Kharissova <sup>1</sup>, Vladimir Zhinzhilo <sup>2</sup>, Julia Bryantseva <sup>2</sup> and Igor Uflyand <sup>2,\*</sup> <sup>1</sup> Universidad Autónoma de Nuevo León, San Nicolás de los Garza 66455, México<sup>2</sup> Department of Chemistry, Southern Federal University, 344090 Rostov-on-Don, Russia

\* Correspondence: iueflyand@sfedu.ru; Tel.: +7-(92)-81112880

**Abstract:** Currently, among the various areas of targeted wastewater treatment, great attention is being given by researchers to the solid-phase extraction of organic dyes using metal–organic frameworks (MOFs). In this work, a mixed-ligand Zr-MOF containing terephthalic acid and 1,10-phenanthroline as linkers was used for this purpose. The limiting adsorption of the dyes Congo red and methylene blue, according to experimental data, is 40 mg/g. The influence of various parameters (time, temperature, adsorbent dosage, pH, and coexisting ions) on adsorption characteristics was studied. The sorbent was tested for the removal of dyes from drinks in water and in artificial seawater. The possibility of the separation of dyes by column chromatography using a sorbent as a filler was studied.

**Keywords:** adsorption; metal–organic frameworks; organic dyes; sorbent; solid-phase extraction



**Citation:** Kharisov, B.; Kharissova, O.; Zhinzhilo, V.; Bryantseva, J.; Uflyand, I. Solid-Phase Extraction of Organic Dyes on Mixed-Ligand Zr(IV) Metal–Organic Framework. *Appl. Sci.* **2022**, *12*, 12219. <https://doi.org/10.3390/app122312219>

Academic Editors: Stephen David Worrall and Julia Linnemann

Received: 1 November 2022

Accepted: 28 November 2022

Published: 29 November 2022

**Publisher's Note:** MDPI stays neutral with regard to jurisdictional claims in published maps and institutional affiliations.



**Copyright:** © 2022 by the authors. Licensee MDPI, Basel, Switzerland. This article is an open access article distributed under the terms and conditions of the Creative Commons Attribution (CC BY) license (<https://creativecommons.org/licenses/by/4.0/>).

## 1. Introduction

Zirconium-based metal–organic frameworks (Zr-MOFs) have become the focus of research in analytical chemistry due to their promising properties, including good selectivity, high performance, low cost, and regeneration, as well as the strong interaction of framework metal centers with functional groups of organic pollutants [1–7]. The strong bonds between the metal and carboxyl groups are responsible for the high stability of Zr-MOF [1,8–10]. As one type of stable MOF, Zr-MOFs show high efficiency in removing dyes [11], antibiotics [12], and heavy metal ions [13].

The disadvantages of Zr-MOFs include low adsorption rates and a long time for the establishment of an equilibrium state. Of the methods for increasing the adsorption capacity, the following should be singled out. Thus, the use of crystallization modulators in the synthesis makes it possible to increase the size of Zr-MOF crystallites by four orders of magnitude (from 10 to 100 μm) [14–18]. Typical modulators are monocarboxylates to bind to metal clusters (coordination modulators) and thus to compete with the linker [14–17], or acidic species to reduce the deprotonation of linkers (protonation modulators) [19]. The stability of such solids is well suited for further study of the effect of functionalization on their properties, and several experimental studies have established the possibility of additionally introducing new functional groups into the structure of these compounds [20].

Among the generally accepted methods of synthesis, including stepwise and bottom-up, the mixed-ligand strategy has become widespread in MOF design [21,22]. The term “mixed ligands” means that two types of linkers with similar spatial architectures or completely different structures are used for MOF synthesis. Regarding ligand attachment, a carboxyl ligand is often used in MOF construction due to the variety of coordination modes, and a polypyridine organic ligand can bind or chelate a metal ion. As an example, the use of a mixed-ligand strategy to produce Zr-MOF, including, in addition to carboxylate ions, various polypyridine ligands such as 2,2'-bipyridine and 1,10-phenanthroline can be mentioned [23–31]. In relation to our study, 1,10-phenanthroline, which has a rather rigid,

flat, geometric structure, is of the greatest interest. In addition, the electron-conjugated heterocyclic aromatic ligand imparts a significant redox inertness to the complex, which favorably distinguishes MOF synthesized by us from those described earlier. The presence of a vacant  $\pi$ -orbital in the phenanthroline molecule makes it possible to expect that the formed mixed-ligand complex will have a significant charge transfer from the metal atom to the ligand, possibly in the visible and UV regions, which was also not previously described for MOFs of this type.

The aim of our study was to use a ligand-mixed Zr-MOF containing terephthalic acid and 1,10-phenanthroline as linkers in the solid-phase extraction (SPE) of organic dyes.

## 2. Materials and Methods

### 2.1. Materials

Zirconium(IV) chloride ( $ZrCl_4$ ), chloroform ( $CHCl_3$ ), ethanol ( $C_2H_6O$ ), methanol ( $CH_4O$ ), hydrochloric acid (HCl),  $N,N'$ -dimethylformamide (DMF), and sodium hydroxide (NaOH) were purchased from Sigma-Aldrich and were used without further purification.

The dyes used as adsorbates were methylene blue (MB), Congo red (CR), and malachite green (MG), with the molecular formulas  $C_{16}H_{18}N_3SCl$ ,  $C_{32}H_{22}N_6Na_2O_6S_2$ , and  $C_{23}H_{25}ClN_2$ , solubility in water of 50, 10, and 110 g/L (20 °C), as well as molecular weights of 319.85, 696.66, and 301.453 g/mol, respectively (Figure 1). They were purchased from Sigma-Aldrich. The original dye solution with a concentration of 200 mg/L was obtained by dissolving an accurate weighed portion of the dye in distilled water. When preparing the experimental solutions, the dye stock solution was diluted in exact proportions to the required initial concentrations.



**Figure 1.** Formulas of Congo red (CR), methylene blue (MB), and malachite green (MG).

### 2.2. Synthesis of Sorbent

The sorbent was synthesized in accordance with the procedure described in the work of [32]. Briefly,  $ZrCl_4$  (3.5 g, 10 mmol), terephthalic acid (4.95 g, 30 mmol), and 1,10-phenanthroline (2.7 g, 15 mmol) were dissolved in DMF. The resulting mixture was sealed into a glass ampoule, which was completely immersed in a vessel with fine calcined sand and heated at 132 °C for 72 h. After that, the ampoule was opened, the resulting precipitate was filtered off, washed with hot DMF, and then with hot ethanol and dried at 60 °C in air. The dried substance was washed in a Soxhlet apparatus with ethyl acetate for 6 h and activated by heating in vacuum at 150 °C for 8 h.

### 2.3. Characterization

A CHNOS vario EL cubic analyzer (Elementar Analysensysteme GmbH, Germany) was used for elemental analysis. An energy-dispersive X-ray fluorescence spectrometer “X-Art M” (Comita, Russia) or atomic absorption spectrometer “MGA-915” (Lumex, Russia) were used to determine the content of zirconium. An AUTOSORB-1 instrument (Quantachrome, Boynton Beach, FL, USA) was used to study nitrogen adsorption/desorption isotherms at 77 K (liquid  $N_2$ ) using the static volumetric method. The samples were degassed by heating at 150 °C for 12 h in a vacuum before the start of the experiments. The calculation of the Brunauer–Emmett–Teller surface area was made from the amount of  $N_2$  physically adsorbed at various  $P/P_0$  ratios based on the linear part of the six-point

adsorption data at  $P/P_0 = 0.02\text{--}0.10$ . The experiments were carried out using ultra-high purity gases (99.995%).

#### 2.4. Solid-Phase Extraction Procedures

In this work, the experiments were carried out using the solid-state extraction of MB, CR, and MG as the main dyes from aqueous solutions using the synthesized sorbent. Solutions of the dyes (200 mL) were placed into a thermostated beaker with a volume of 300 mL at temperatures of 10, 18, and 35 °C. After the specified temperature was reached, the sorbent (0.1 g) was added, and 10 mL of the sorbent suspension was taken from the dye solution every 5, 10, 15, 30, 45, and 60 min, followed by centrifugation for 5 min at 4500 rpm. The concentration of the residual dye in the fugate was determined at  $\lambda_{\max}$  492 nm (CR) [33] or 664 nm (MB) [34] on a UV-visible spectrophotometer (Varian, Cary 50).

The removal efficiency  $R$  (%) was calculated from Equation (1):

$$R = \frac{(C_0 - C_t)}{C_0} \times 100\% \quad (1)$$

where  $C_0$  is the initial concentration and  $C_t$  is the dye concentration at time  $t$ .

The equilibrium adsorption  $q_e$  (mg/g) was calculated using Equation (2):

$$q_e = \frac{(c_0 - c_e)V}{m} \quad (2)$$

where  $V$  is the volume of the adsorbate solution (L) and  $m$  is the weight of the adsorbent (g).

The pseudo first-order adsorption model can be expressed by Equation (3) [35]:

$$\frac{dq}{dt} = k_1(q_e - q_t) \quad (3)$$

where  $k_1$  ( $\text{min}^{-1}$ ) is the rate constant of the pseudo first-order model.

After a definite integration, Equation (3) takes the form:

$$\ln(q_e - q_t) = \ln q_e - k_1 t \quad (4)$$

The constant  $k_1$  can be experimentally determined from the slope of the linear plots  $\ln(q_e - q_t)$  versus  $t$ .

The effect of pH on dye adsorption was studied in solutions with pH 3–11. The residual dye concentration was determined after shaking the dye suspension for 120 min at 18 °C until equilibrium was reached, followed by filtration through membrane filters with a pore size of 0.2  $\mu\text{m}$ .

The adsorption isotherms were calculated in accordance with the linearized Equations of Langmuir (5) and Freundlich (6).

$$\frac{1}{q_e} = \frac{1}{q_{\max} K_L c_e} + \frac{1}{q_{\max}} \quad (5)$$

$$\ln q_e = \ln K_F + \frac{1}{n_F} \ln c_e \quad (6)$$

The thermodynamic parameters of adsorption  $\Delta G^0$ ,  $\Delta H^0$ , and  $\Delta S^0$  are calculated graphically from the dependence of  $\ln K_d$  on  $1/T$ , where  $K_d$  is the adsorbate distribution coefficient, calculated by Equation (7) [36]:

$$K_d = \frac{C_0 - C_e}{C_e} \cdot \frac{V}{m} \quad (7)$$

### 3. Results and Discussion

#### 3.1. Synthesis and Characterization of the Sorbent

In this work, a sorbent was synthesized using the solvothermal method by reacting  $ZrCl_4$ , terephthalic acid, and 1,10-phenanthroline in DMF. Based on the literature data and the results obtained in the work, we can assume the following structure of the synthesized compound (Figure 2).

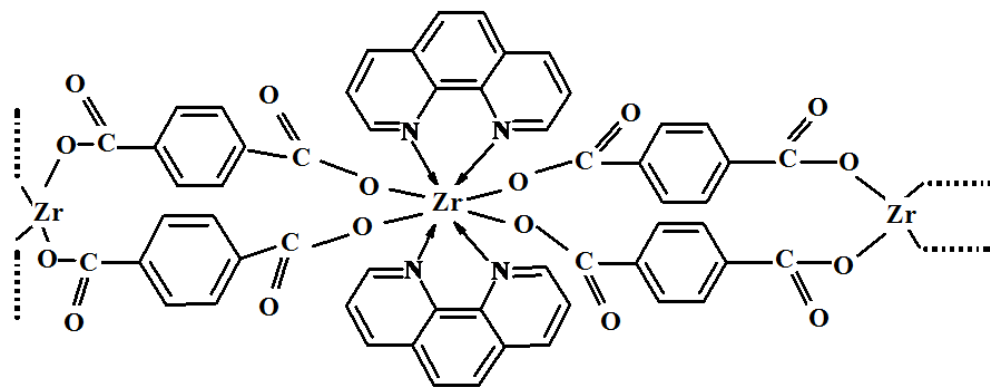


Figure 2. Plausible structure of the sorbent.

The obtained  $N_2$  adsorption–desorption isotherms at 77 K and the pore size distribution for the synthesized MOF are shown in Figure 3. The analysis of nitrogen physisorption isotherms shows that MOF has a constant porosity and a mesoporous structure with a large surface area corresponding to adsorption type II. These characteristics are typical of high-quality MOF material with little pore collapse and no residual reagent. A high nitrogen adsorption of  $561 \text{ cm}^3/\text{g}$  at 77 K was determined for the MOF sample with a pore size of  $9.6 \text{ \AA}$ . The presence of a pronounced hysteresis loop (Figure 3A) makes it possible to attribute the obtained isotherm to type IV according to the IUPAC classification and indicates that mesopores are present along with micropores [37].

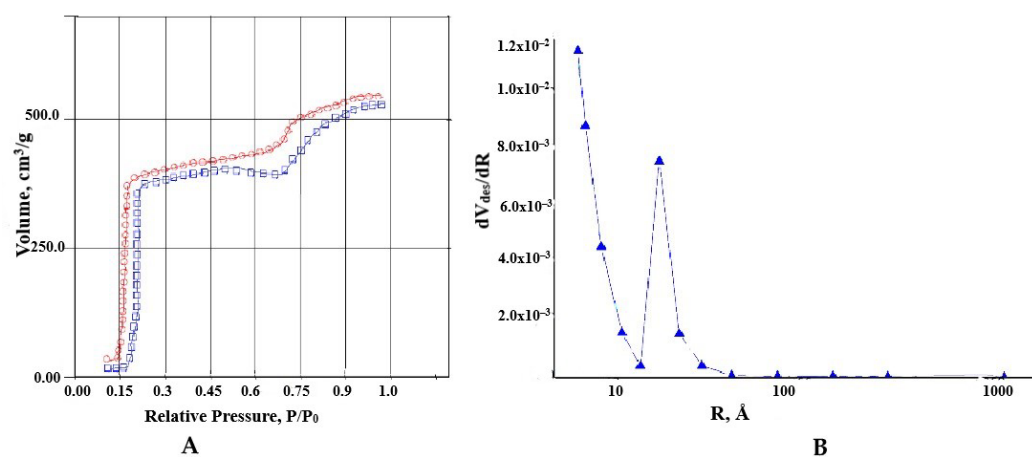


Figure 3.  $N_2$  adsorption–desorption isotherms (A) and the pore size distribution curve (B) for MOF.

#### 3.2. Solid-Phase Extraction of Organic Dyes

To determine the adsorption of CR and MB from their aqueous solutions by the synthesized sorbent, we used the method described in [38]. The effect of pH of the sample solution, the amount of adsorbent, and the adsorption time on the removal efficiency was studied. The results are shown in Figure 4. In the initial period, the adsorption capacity of the sorbent increases rapidly, and then significantly decreases with increasing adsorption time. First, diffusion to the outer surface occurs, accompanied by diffusion into the pores

of the sorbent, because of which equilibrium is quickly achieved. The limiting adsorption, according to the experimental data, is 40 mg/g.

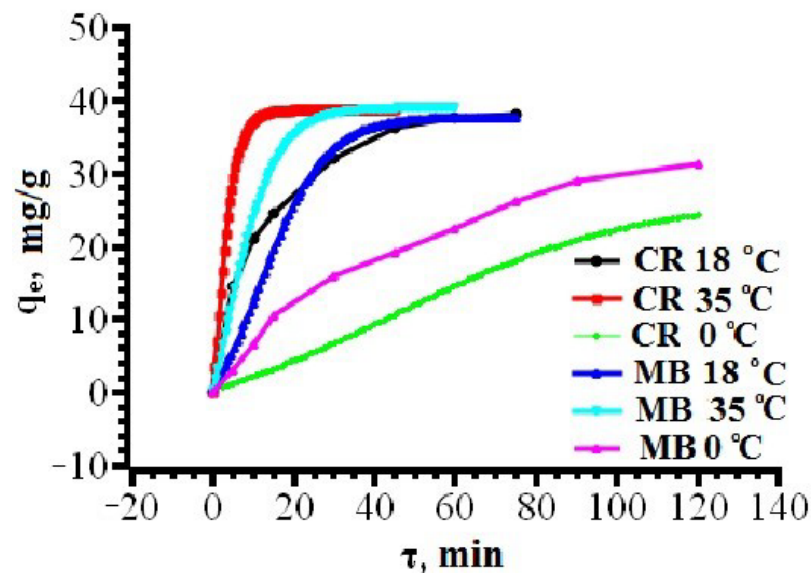


Figure 4. Dependence of adsorption on time.

The temperature dependence of the removal efficiency at pH = 7 is shown in Figure 5. It turned out that an increase in the temperature leads to a more rapid achievement of adsorption equilibrium and the limiting degree of removal is reached within 20 min.

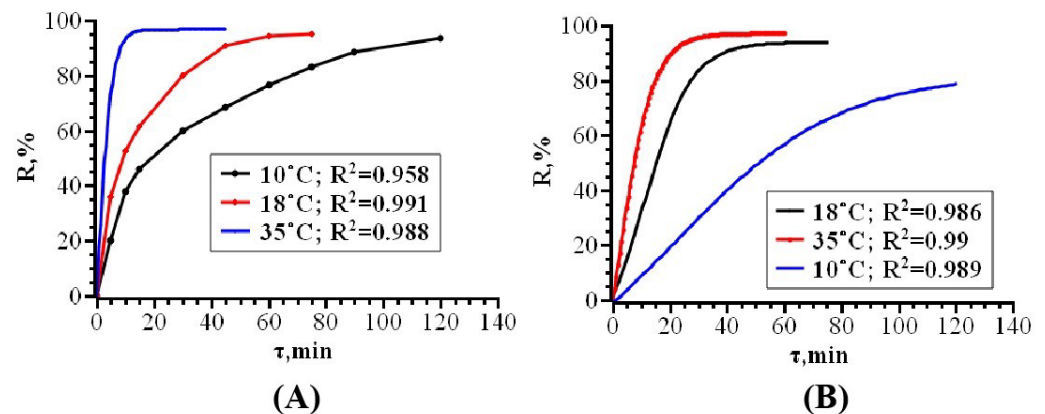
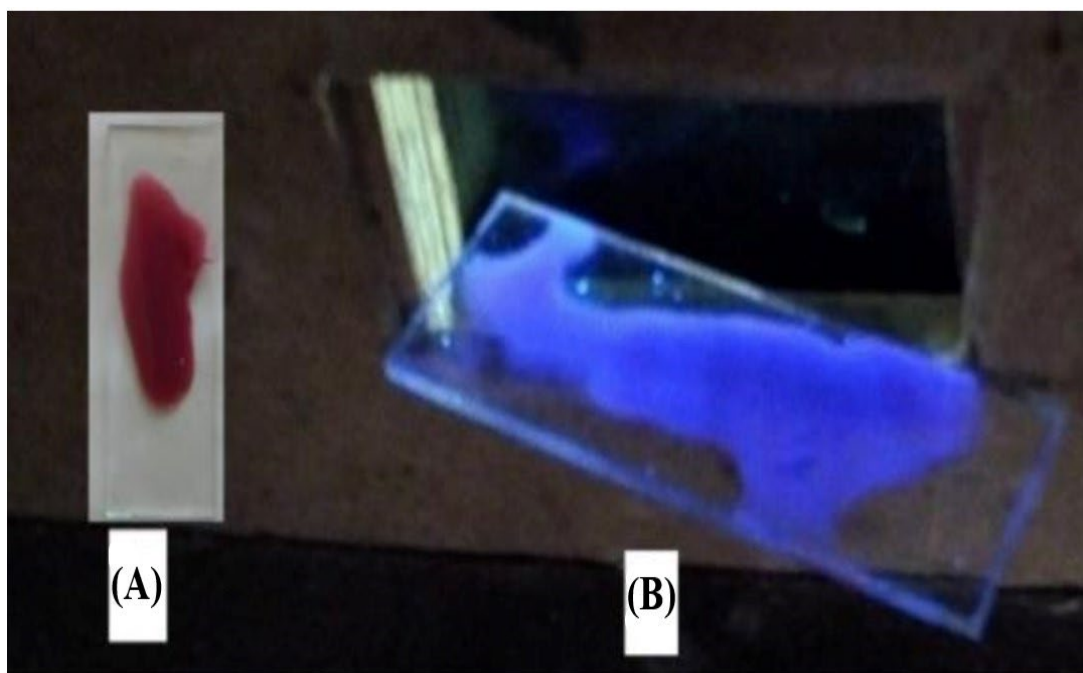


Figure 5. Dependence of removal efficiency on time at different temperatures: (A)—CR, (B)—MB.

The resulting product of the SPE of CR and the synthesized sorbent luminesces in blue when irradiated with UV light with a wavelength of 385 nm, which may indicate that a  $\pi$ - $\pi$  interaction occurs between the dye molecule and the adsorbent during the extraction process (Figure 6) [39].



**Figure 6.** Appearance of the SPE product of CR: (A)—in daylight and (B)—in ultraviolet light ( $\lambda = 385 \text{ nm}$ ).

Based on the results of the study, it can be concluded that the sorbent effectively removes the CR dye from an aqueous solution at a temperature of  $35 \text{ }^{\circ}\text{C}$ . However, at a temperature of  $18 \text{ }^{\circ}\text{C}$ , this complex was not effective enough. When extracting MB food coloring with a sorbent in an aqueous solution, the opposite situation is observed. A more efficient extraction is observed at a temperature of  $18 \text{ }^{\circ}\text{C}$  with a short-term increase in the first 10 min, at which, apparently, the substance activation process occurs, since after 15 min, the concentration of the MB dye sharply decreased from  $25.8 \text{ mg/L}$  to  $0.4 \text{ mg/L}$ . Thus, after 15 min, the concentration of the dye decreased by 64.5 times, and after 60 min, by 7500 times, which indicates a high efficiency of the sorbent in the extraction of the MB dye at room temperature.

When the dye is extracted at a temperature of  $35 \text{ }^{\circ}\text{C}$ , the moment of activation is also present, but it is shifted and appears after 30 min. In the period from 30 min to 45 min, the concentration of the food coloring MB in an aqueous solution decreases from  $16.8 \text{ mg/L}$  to  $4.4 \text{ mg/L}$ , that is, almost four times. This indicates the effectiveness of using the sorbent, but not as effective as at room temperature.

The study of the effect of acidity was carried out in the pH range 3–11. We have found that the degree of MB removal is practically independent of the pH of the medium in this range, while for CR, this dependence is quite significant (Figures 7 and 8).

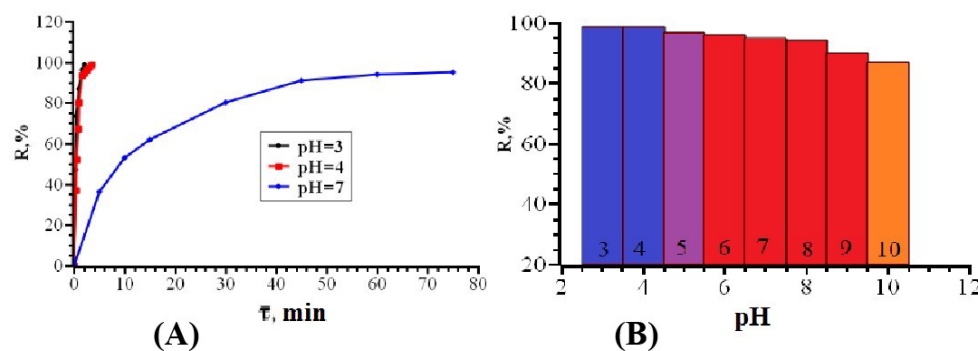


**Figure 7.** Dependence of the dye removal efficiency on time at different pH (A) and on pH (B).

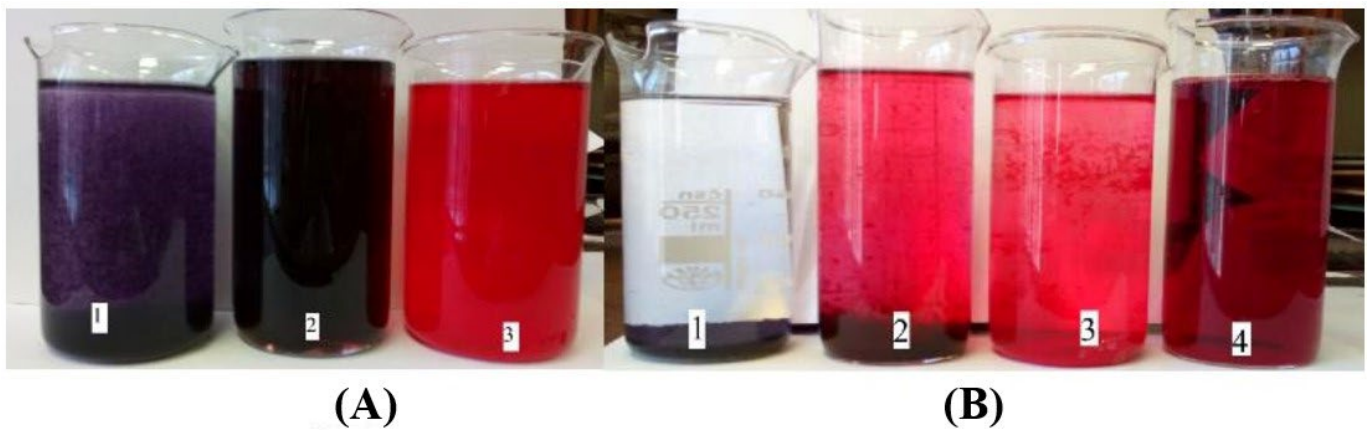


**Figure 8.** Dependence of the removal efficiency of CR from an aqueous solution on pH. (A)—CR solution after 1 min of extraction at pH = 3 (1), 7 (2), and 11 (3). (B)—CR solution one day after reaching equilibrium of the solid-phase extraction at pH = 3 (1), 7 (2), and 11 (3). (4)—Initial solution.

To describe the adsorption of dyes using the synthesized sorbent, a pseudo first-order kinetic model was used, the compliance of which was confirmed by regression analysis using the least squares method (Figure 9). The pseudo first-order adsorption rate constants calculated by the graphical method are shown in Table 1.

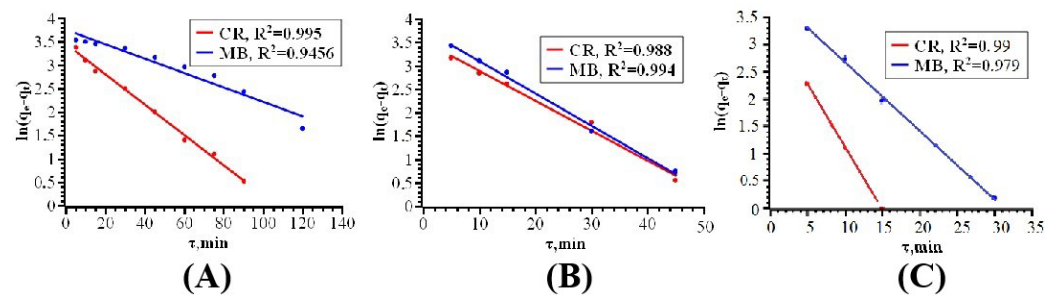


**Figure 9.** Kinetic model of adsorption in linearized form at 283 (A), 291 (B), and 308 K (C).

**Table 1.** Best fit parameters for the dye adsorption onto the sorbent by the Langmuir and Freundlich models.

Dyes	T [K]	Pseudo First-Order Kinetics		Langmuir Model		Freundlich Model	
		Constant $k_1$ [min <sup>-1</sup> ]		$K_L$ [L/mg]	$R^2$	$K_F$ [mg <sup>-1/n</sup> L <sup>1/n</sup> g <sup>-1</sup> ]	$R^2$
CR	283	0.0173		0.93	0.996	3.17	0.912
	291	0.0555		2.16	0.991	4.12	0.956
	308	0.317		3.12	0.998	5.4	0.974
MB	283	0.078		0.85	0.895	2.76	0.889
	291	0.08		1.96	0.981	3.94	0.954
	308	0.082		2.74	0.915	4.22	0.963

The Langmuir and Freundlich adsorption isotherms of dyes using a sorbent are shown in Figures 10 and 11, and Table 1 shows the coefficients of these isotherms. Most of the  $R^2$  values are greater than 0.9 for all isotherm models. The  $R_L$  values for the Langmuir adsorption of the dye on the sorbent were between 0 and 1, indicating favorable adsorption. The  $K_L$  values (0.93, 2.16, and 3.12 L mg<sup>-1</sup> at 283, 291, and 308 K, respectively) indicate an increase in dye adsorption on the sorbent with increasing temperature. The  $K_F$  and  $1/n$  values increase and decrease with increasing temperature, respectively. The  $1/n$  values were between 0 and 1, indicating favorable adsorption.

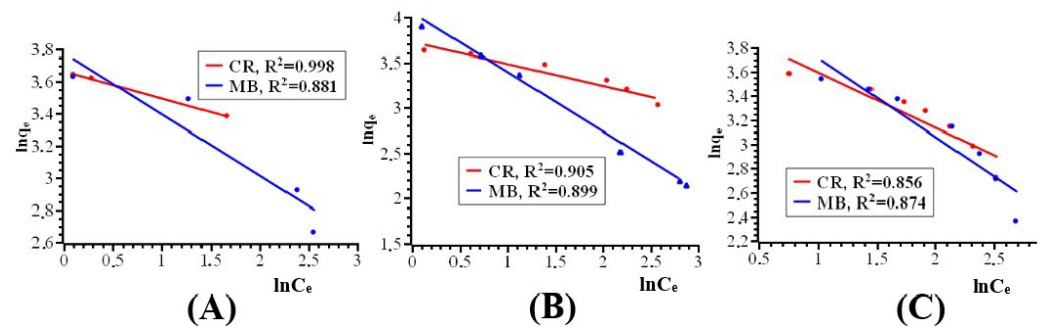


Figure 10. Freundlich isotherms in linearized form at 283 (A), 291 (B), and 308 K (C).

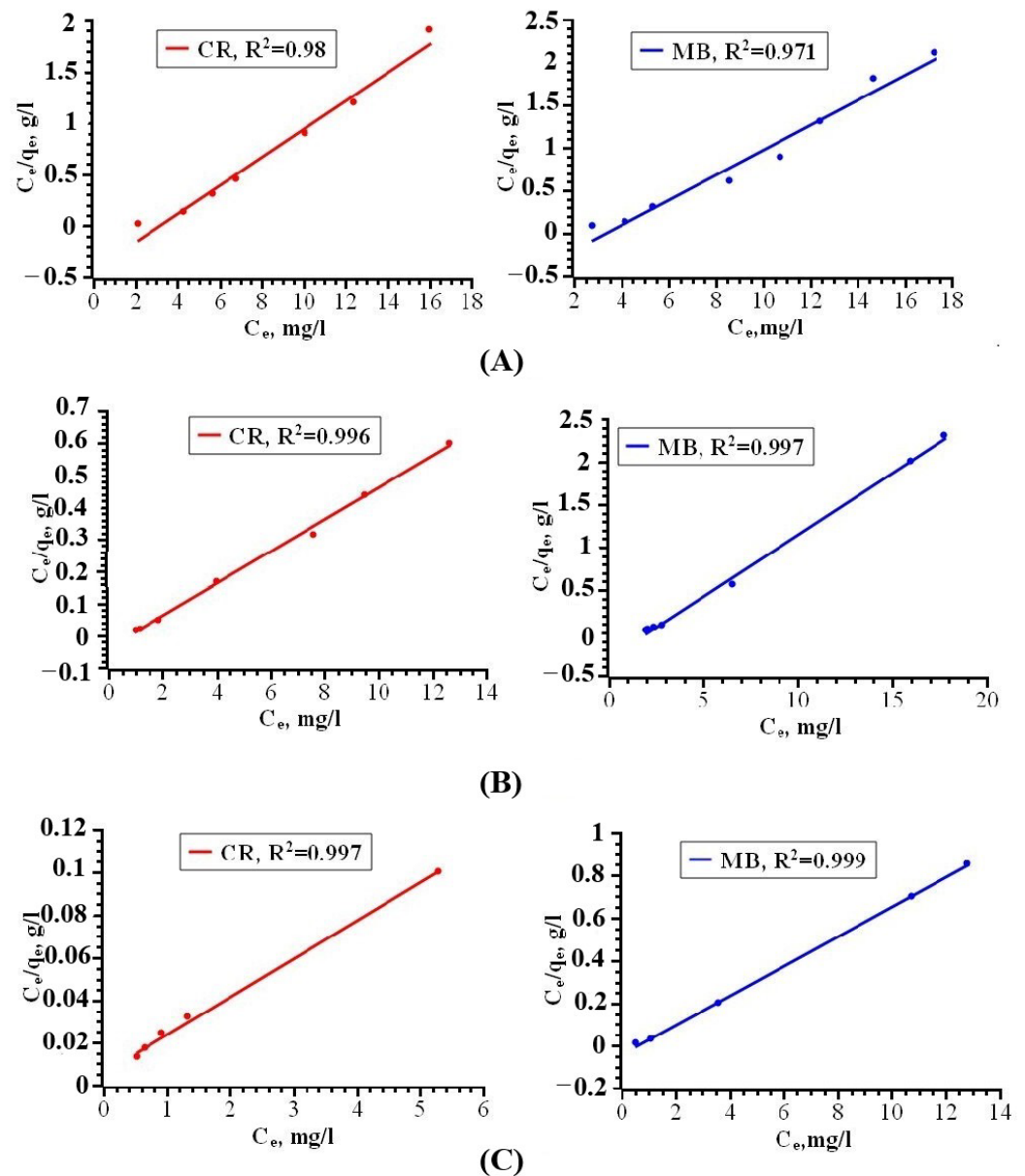
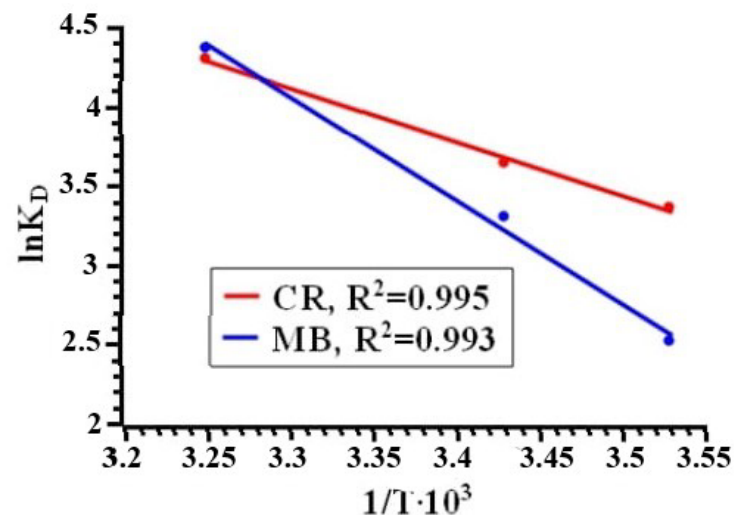


Figure 11. Langmuir isotherms of CR and MV at 283 (A), 291 (B), and 308 K (C).

The calculated values of  $K_D$  are presented in Table 2 and the dependence of the distribution constant on the reciprocal temperature (Figure 12) was used to calculate the thermodynamic parameters.

**Table 2.** Calculated values of  $K_d$ .

Dyes	T [°C]	$K_D$
CR	283	$2.4 \cdot 10^4$
MB	283	$3.5 \cdot 10^3$
CR	291	$3.2 \cdot 10^4$
MB	291	$1.5 \cdot 10^4$
CR	308	$4.9 \cdot 10^4$
MB	308	$1.9 \cdot 10^4$

**Figure 12.** Dependence of the distribution constant on the reciprocal temperature.

As shown in Table 3, the negative values of  $\Delta G^0$  at temperatures of 283, 291, and 308 K indicate the spontaneous nature of the adsorption process.  $\Delta G^0$  decreases with an increase in the temperature, which indicates more efficient adsorption at a higher temperature. In addition, a positive  $\Delta S^0$  value indicates an increase in the degrees of freedom at the solid–liquid interface during the adsorption of dyes on the sorbent and reflects the affinity of the sorbent for dye ions in aqueous solutions and may indicate some structural changes in the adsorbents.

**Table 3.** Thermodynamic parameters for the adsorption of the dyes on the sorbent.

Dyes	$\Delta G^0$ [kJ/mol]			$\Delta H^0_{283}$ [kJ/mol]	$\Delta S^0_{283}$ [J/mol K]
	283 K	291 K	308 K		
MB	−7.9	−8.8	−11	−57	17.3
CR	−5.9	−8.8	−11.16	−65	20.8

### 3.3. Solid-Phase Extraction of Dyes in Real Samples

Although dyes improve the appearance of food products, they significantly affect their safety. Therefore, an important problem in the use of dyes in food is the threat to human health due to the accumulation of dyes in food [40,41]. To test the reliability of a sorbent for removing artificial dyes from a sample of a food product, which is the low-alcohol drink “Cherry”, experiments were carried out to study the kinetics and adsorption isotherm. The drink contains the dye carmosine (azorubine) E-122 (Figure 13) and natural cherry juice.

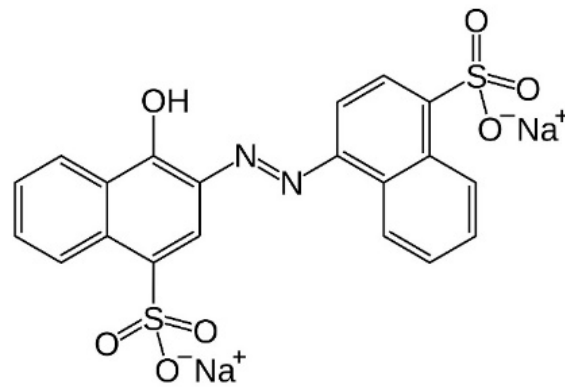


**Figure 13.** Formula of carmosine.

To identify the dyes that make up the drink, we took a UV–vis absorption spectrum. In Figure 14, there is an absorption band characteristic of carmosine in the region of 516 nm, the intensity of which decreases depending on the time of contact with the sorbent [42,43].

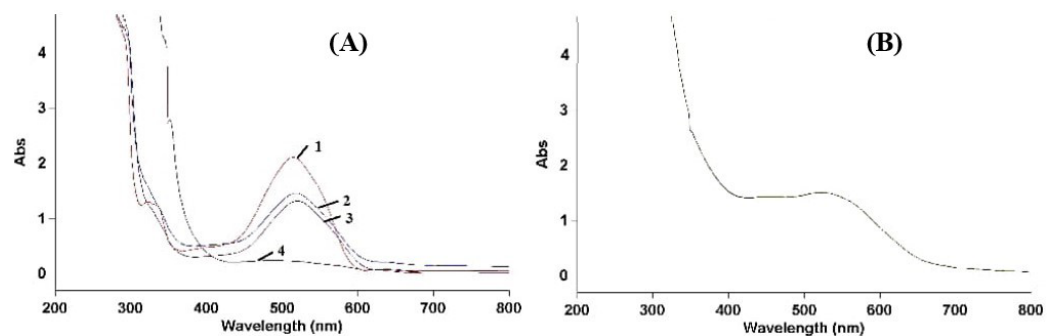


**Figure 14.** UV–vis absorption spectra (A) of the drink before extraction (1) and 30 (2), 45 (3), and 120 min (4) after the start of extraction. (B)—UV–vis absorption spectrum of anthocyanin.

The characteristic absorption band (Figure 14B) corresponding to the natural anthocyanin of the cherry, represented by the two compounds cyanidin-3-glucosylrutinosid (Cy-3-GR) and cyanidin-3-rutinosid (Cy-3-R) (Figure 15), was not detected. Figure 16 shows the dynamics of SPE of MB with an absorption maximum at 664 nm.

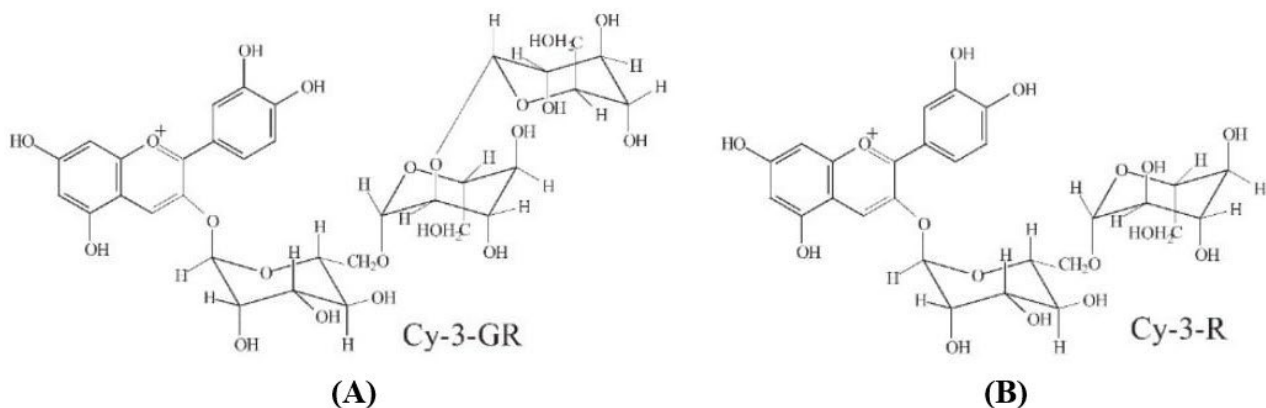


**Figure 15.** Structures of anthocyanins: (A)—cyanidin-3-glucosylrutinosid (Cy-3-GR) and (B)—cyanidin-3-rutinosid (Cy-3-R), characteristic of cherry fruits.

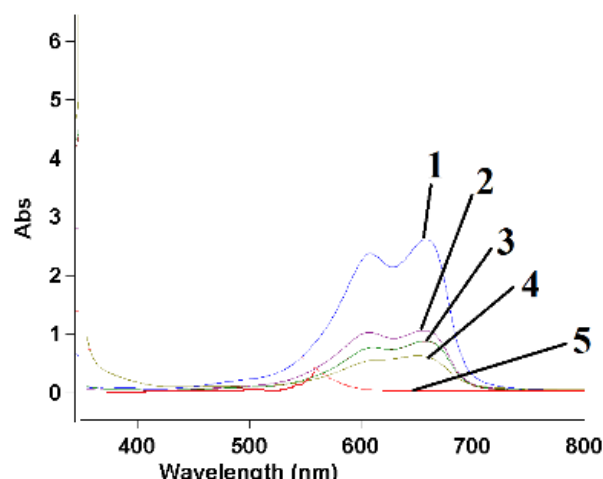


**Figure 16.** UV-vis absorption spectra of the solution before processing with the sorbent (1) and 15 (2), 30 (3), 45 (4), and 60 min (5) after SPE.

### 3.4. Solid-Phase Extraction of Dyes in Artificial Seawater

Today, the marine environment is becoming more and more polluted due to the release of dangerous dyes into it. Therefore, we studied the adsorption characteristics of the sorbent in artificial seawater. The method of making artificial seawater belongs to the Khan scheme [44]. The Lyman and Fleming formula (Table 4) was used to prepare an artificial seawater solution by dissolving analytical-grade reagents in bi-distilled water.

**Table 4.** Chemical composition of artificial seawater.

Salt	Content [g/kg]
NaCl	23.476
KCl	0.664
CaCl <sub>2</sub>	1.102
MgCl <sub>2</sub>	4.981
Na <sub>2</sub> SO <sub>4</sub>	3.917
NaHCO <sub>3</sub>	0.192
KBr	0.096
SrCl <sub>2</sub>	0.025
NaF	0.003
H <sub>3</sub> BO <sub>3</sub>	0.027

Salinity was 34.481%; pH was adjusted to 7.5, 8, 8.2, and 8.5 with sodium hydroxide (NaOH) or hydrochloric acid (HCl).

The method for studying the adsorption in artificial seawater is similar to the method described above for studying in ideal water. The adsorption characteristics of the sorbent in artificial seawater deteriorate somewhat (Figure 17). The presence of various inorganic salts in artificial seawater has less effect on the adsorption of a low-concentration dye solution compared to a high-concentration dye solution. The decrease in the adsorption capacity of the sorbent in artificial seawater compared to an ideal aqueous solution is only 3–6%. A decrease in the adsorption capacity is associated with a deterioration in the solubility of dyes after the addition of various inorganic salts to the solution [45] and the competition of SO<sub>4</sub><sup>2-</sup>, Cl<sup>-</sup>, F<sup>-</sup>, etc., ions with dye molecules for unsaturated sites on adsorbents [46,47].

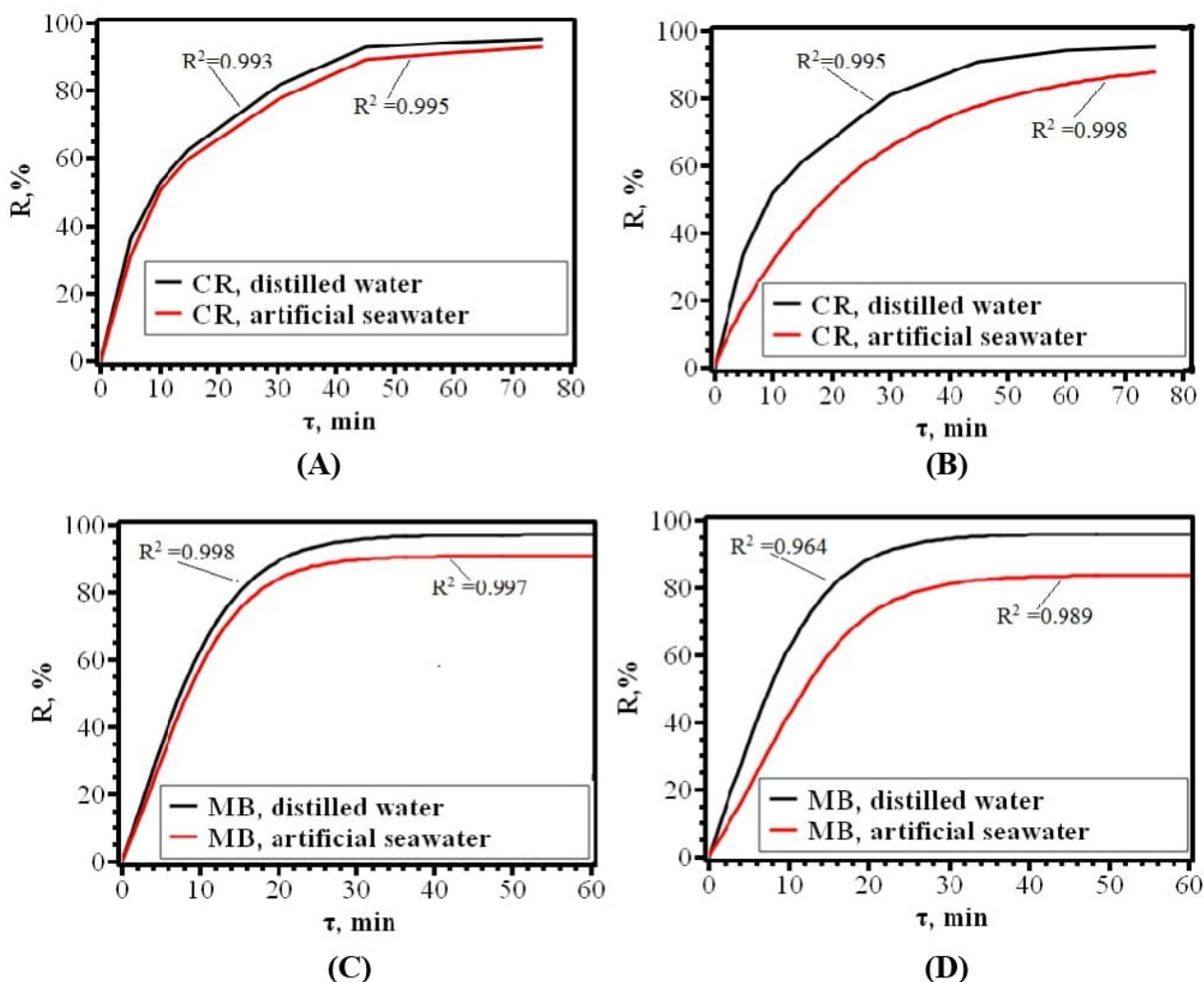


**Figure 17.** Removal efficiency of CR and MB from distilled water and artificial seawater at 293 K at a concentration of  $20 \text{ mg L}^{-1}$  (A,C) and  $40 \text{ mg L}^{-1}$  (B,D).

### 3.5. Sorbent as a Filler for Column Chromatography for Dye Separation

Based on the excellent adsorption characteristics of dyes on the sorbent and considering the previously obtained results [48,49], we used it as the stationary phase of the chromatographic column. The chromatographic column consists of a glass tube that has been filled with a sorbent as a stationary phase. A mixed solution of MB, MG, and CR was injected into the chromatographic column at the same concentration, respectively. As shown in Figure 18, CR was adsorbed to the stationary phase for a long time along with the eluent flow, while MB and MG passed through the column. In the upper part of the photo, there is a concentrated mixture of MG and MB, while the CR adsorbed on the sorbent is in the lower part. The results obtained indicate the possibility of the separation of dyes by passing through a chromatographic column, which can be easily seen with the naked eye. These experiments highlight the potential of the sorbent as a filler for column chromatography to separate dyes.

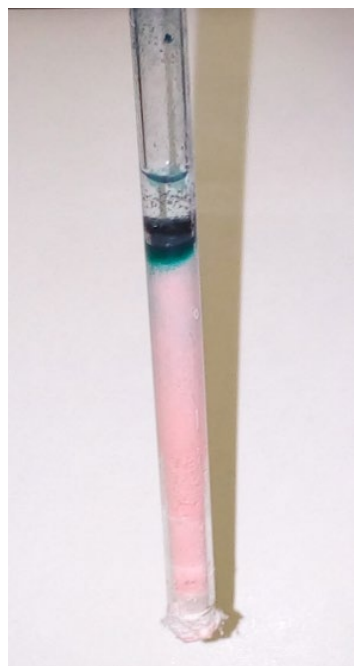


**Figure 18.** Selective separation of a mixture of dyes (methylene blue, malachite green, and Congo red) on a column filled with the studied sorbent.

#### 4. Conclusions

In summary, a ligand-mixed Zr(IV)-MOF based on terephthalic acid and 1,10-phenanthroline is a promising sorption material for the solid-phase extraction of organic pollutants (synthetic dyes), demonstrating a high efficiency of removing the target pollutant. The adsorption behavior has been investigated in terms of several important parameters, including adsorption kinetics, isotherms, and initial pH. The results showed that the maximum adsorption capacity of MOF reached 40 mg/g. Moreover, it has been used in practice in food samples and has shown high performance. The excellent performance of this sorbent in artificial seawater makes it a promising material for seawater treatment. Potentially, it can serve as a filler for column chromatography to separate dye molecules. The sorbent studied favorably differs from the sorbents described earlier in the literature by its versatility, since it shows good adsorption qualities with respect to both cationic and anionic dyes. The complex can also be used to extract neutral dyes using solid-phase extraction. The extraction of dyes occurs in a wide pH range of the medium and under conditions of solutions with high ionic strength (seawater). Selecting the conditions for elution, one can achieve the selective separation of dyes, which favorably distinguishes this compound from the sorbents described earlier in the literature.

**Author Contributions:** Conceptualization, I.U. and B.K.; methodology, I.U., B.K. and O.K.; writing—original draft, I.U.; writing—review and editing, I.U. and B.K.; investigation, V.Z., J.B. and O.K.; visualization, J.B., supervision, I.U. All authors have read and agreed to the published version of the manuscript.

**Funding:** This research received no external funding.

**Institutional Review Board Statement:** Not applicable.

**Informed Consent Statement:** Not applicable.

**Data Availability Statement:** Not applicable.

**Conflicts of Interest:** The authors declare no conflict of interest.

## References

1. Cavka, J.H.; Jakobsen, S.; Olsbye, U.; Guillou, N.; Lamberti, C.; Bordiga, S.; Lillerud, K.P. A new zirconium inorganic building brick forming metal organic frameworks with exceptional stability. *J. Am. Chem. Soc.* **2008**, *130*, 13850–13851. [[CrossRef](#)] [[PubMed](#)]
2. Butova, V.V.; Soldatov, M.A.; Guda, A.A.; Lomachenko, K.A.; Lamberti, C. Metal-organic frameworks: Structure, properties, methods of synthesis and characterization. *Russ. Chem. Rev.* **2016**, *85*, 280–307. [[CrossRef](#)]
3. Tsivadze, A.Y.; Knyazeva, M.K.; Solovtsova, O.V.; Men'Shchikov, I.E.; Fomkin, A.A.; Shkolin, A.V.; Khozina, E.V.; Grachev, V.A.; Aksyutin, O.E.; Ishkov, A.G. Metal-organic framework structures: Adsorbents for natural gas storage. *Russ. Chem. Rev.* **2019**, *88*, 925–978. [[CrossRef](#)]
4. Solovtsova, O.V.; Pulin, A.L.; Men'shchikov, I.E.; Platonova, N.P.; Knyazeva, M.K.; Chugaev, S.S.; Shkolin, A.V.; Fomkin, A.A. Zr-based metal-organic nanoporous adsorbents of high density for methane storage. *Prot. Met. Phys. Chem. Surf.* **2020**, *56*, 1114–1121. [[CrossRef](#)]
5. Pribylov, A.A.; Murdmaa, K.O.; Solovtsova, O.V. Methane adsorption on the Zr-BDC metal-organic framework structure at supercritical temperatures and pressures. *Russ. Chem. Bull.* **2021**, *70*, 665–671. [[CrossRef](#)]
6. Uflyand, I.E.; Zhinzhiro, V.A.; Nikolaevskaya, V.O.; Kharisov, B.I.; Oliva González, C.M.; Kharissova, O.V. Recent Strategies to Improve MOF Performance in Solid Phase Extraction of Organic Dyes. *Microchem. J.* **2021**, *168*, 106387. [[CrossRef](#)]
7. Bai, Y.; Dou, Y.; Xie, L.H.; Rutledge, W.; Li, J.R.; Zhou, H.C. Zr-based metal-organic frameworks: Design, synthesis, structure, and applications. *Chem. Soc. Rev.* **2016**, *45*, 2327–2367. [[CrossRef](#)]
8. Wu, H.; Yildirim, T.; Zhou, W. Exceptional Mechanical Stability of Highly Porous Zirconium Metal-Organic Framework UiO-66 and Its Important Implications. *J. Phys. Chem. Lett.* **2013**, *4*, 925–930. [[CrossRef](#)]
9. Howarth, A.J.; Liu, Y.; Li, P.; Li, Z.Z.; Wang, T.C.; Hupp, J.T.; Farha, O.K. Chemical, thermal and mechanical stabilities of metal-organic frameworks. *Nat. Rev. Mater.* **2016**, *1*, 15018. [[CrossRef](#)]
10. Schaate, A.; Roy, P.; Godt, A.; Lippke, J.; Waltz, F.; Wiebcke, M.; Behrens, P. Modulated synthesis of Zr-based metal-organic frameworks: From nano to single crystals. *Chem.–Eur. J.* **2011**, *17*, 6643–6651. [[CrossRef](#)]
11. Molavi, H.; Hakimian, A.; Shojaei, A.; Raeeszadeh, M. Selective dye adsorption by highly water stable metal-organic framework: Long term stability analysis in aqueous media. *Appl. Surf. Sci.* **2018**, *445*, 424–436. [[CrossRef](#)]
12. Chen, C.; Chen, D.; Xie, S.; Quan, H.; Luo, X.; Guo, L. Adsorption behaviors of organic micropollutants on zirconium metal-organic framework UiO-66: Analysis of surface interactions. *ACS Appl. Mater. Interfaces* **2017**, *9*, 41043–41054. [[CrossRef](#)] [[PubMed](#)]
13. He, T.; Zhang, Y.-Z.; Kong, X.-J.; Yu, J.; Lv, X.-L.; Wu, Y.; Guo, Z.-J.; Li, J.-R. Zr(IV)-based metal-organic framework with T-shaped ligand: Unique structure, high stability, selective detection, and rapid adsorption of  $\text{Cr}_2\text{O}_7^{2-}$  in water. *ACS Appl. Mater. Interfaces* **2018**, *10*, 16650–16659. [[CrossRef](#)] [[PubMed](#)]
14. Valenzano, L.; Civalieri, B.; Chavan, S.; Bordiga, S.; Nilsen, M.H.; Jakobsen, S.; Lillerud, K.P.; Lamberti, C. Disclosing the Complex Structure of UiO-66 Metal Organic Framework: A Synergic Combination of Experiment and Theory. *Chem. Mater.* **2011**, *23*, 1700–1718. [[CrossRef](#)]
15. Wißmann, G.; Schaate, A.; Lilienthal, S.; Bremer, I.; Schneider, A.M.; Behrens, P. Modulated synthesis of Zr-fumarate MOF. *Microporous Mesoporous Mater.* **2012**, *152*, 64–70. [[CrossRef](#)]
16. Gutov, O.V.; Molina, S.; Escudero-Adan, E.C.; Shafir, A. Modulation by Amino Acids: Toward Superior Control in the Synthesis of Zirconium Metal-Organic Frameworks. *Chem.–Eur. J.* **2016**, *22*, 13582–13587. [[CrossRef](#)]
17. Marshall, R.J.; Hobday, C.L.; Murphie, C.F.; Griffin, S.L.; Morrison, C.A.; Moggach, S.A.; Forgan, R.S. Amino acids as highly efficient modulators for single crystals of zirconium and hafnium metal-organic frameworks. *J. Mater. Chem. A* **2016**, *4*, 6955–6963. [[CrossRef](#)]
18. Shearer, G.C.; Chavan, S.; Bordiga, S.; Svelle, S.; Olsbye, U.; Lillerud, K.P. Defect Engineering: Tuning the Porosity and Composition of the Metal-Organic Framework UiO-66 via Modulated Synthesis. *Chem. Mater.* **2016**, *28*, 3749–3761. [[CrossRef](#)]
19. Katz, M.J.; Brown, Z.J.; Colon, Y.J.; Siu, P.W.; Scheidt, K.A.; Snurr, R.Q.; Hupp, J.T.; Farha, O.K. A facile synthesis of UiO-66, UiO-67 and their derivatives. *Chem. Commun.* **2013**, *49*, 9449–9451. [[CrossRef](#)]
20. Garibay, S.J.; Cohen, S.M. Isoreticular synthesis and modification of frameworks with the UiO-66 topology. *Chem. Commun.* **2010**, *46*, 7700–7702. [[CrossRef](#)]
21. Dzhardimalieva, G.I.; Uflyand, I.E. Design and synthesis of coordination polymers with chelated units and their application in nanomaterials science. *RSC Adv.* **2017**, *7*, 42242–42288. [[CrossRef](#)]
22. Yang, Y.; Ren, G.; Li, W.; Gu, D.; Liang, Z.; Liu, Y.; Pan, Q. Three coordination complexes based on mixed ligand strategy: Coordination diversities and nitrobenzene detections. *Polyhedron* **2020**, *185*, 114599. [[CrossRef](#)]
23. Feng, X.; Ren, Y.; Jiang, H. Metal-bipyridine/phenanthroline-functionalized porous crystalline materials: Synthesis and catalysis. *Coord. Chem. Rev.* **2021**, *438*, 213907. [[CrossRef](#)]
24. Uflyand, I.E.; Zhinzhiro, V.A.; Dzhardimalieva, G.I.; Knerelman, E.I.; Davydova, G.I.; Shunina, I.G. Synthesis and Properties of Copper Trimesinate Complexes with Polypyridine Ligands. *Russ. J. Gen. Chem.* **2020**, *90*, 1884–1891. [[CrossRef](#)]
25. Qiu, L.-G.; Gu, L.-N.; Hu, G.; Zhang, L.-D. Synthesis, structural characterization and selectively catalytic properties of metal-organic frameworks with nano-sized channels: A modular design strategy. *J. Solid State Chem.* **2009**, *182*, 502–508. [[CrossRef](#)]
26. Dun, L.; Zhang, B.; Wang, J.; Wang, H.; Chen, X.; Li, C. Crystal Structure, Synthesis and Luminescence Sensing of a Zn(II) Coordination Polymer with 2,5-Dihydroxy-1,4-Terephthalic Acid and 2,2'-Bipyridine as Ligands. *Crystals* **2020**, *10*, 1105. [[CrossRef](#)]

27. Yang, B.-P.; Zeng, H.-Y.; Mao, J.-G.; Guo, G.-C.; Huang, J.-S.; Dong, Z.-C. Solvothermal synthesis and crystal structures of two new copper(II) terephthalates. *Transition Met. Chem.* **2003**, *28*, 600–605. [[CrossRef](#)]
28. Yang, Z.; Cao, J.; Chen, Y.; Li, X.; Xiong, W.; Zhou, Y.; Zhou, C.; Xu, R.; Zhang, Y. Mn-doped zirconium metal-organic framework as an effective adsorbent for removal of tetracycline and Cr(VI) from aqueous solution. *Microporous Mesoporous Mater.* **2019**, *277*, 277–285. [[CrossRef](#)]
29. Xu, H.; Liang, Y.; Su, Z.; Zhao, Y.; Shao, K.; Zhang, H.; Yue, S. Tetraaqua(2,2'-bipyridine)zinc(II) terephthalate. *Acta Cryst.* **2004**, *E60*, m142–m144. [[CrossRef](#)]
30. Go, Y.; Wang, X.; Anokhina, E.V.; Jacobson, A.J. A Chain of Changes: Influence of Noncovalent Interactions on the One-Dimensional Structures of Nickel(II) Dicarboxylate Coordination Polymers with Chelating Aromatic Amine Ligands. *Inorg. Chem.* **2004**, *43*, 5360–5367. [[CrossRef](#)]
31. Go, Y.B.; Wang, X.; Anokhina, E.V.; Jacobson, A.J. Influence of the Reaction Temperature and pH on the Coordination Modes of the 1,4-Benzenedicarboxylate (BDC) Ligand: A Case Study of the NiII(BDC)/2,2'-Bipyridine System. *Inorg. Chem.* **2005**, *44*, 8265–8271. [[CrossRef](#)]
32. Kharissova, O.V.; Zhinzhiro, V.A.; Bryantseva, J.D.; Uflyand, I.E.; Kharisov, B.I. Zr<sup>IV</sup> metal-organic framework based on terephthalic acid and 1,10-phenanthroline as adsorbent for solid-phase extraction of tetracycline antibiotics. *Mendeleev Commun.* **2022**, *32*, 661–663. [[CrossRef](#)]
33. Abo-State, M.A.M.; Saleh, Y.E.; Hazaa, H.A. Decolorization of Congo Red dye by bacterial isolates. *J. Ecol. Health Environ.* **2017**, *5*, 41–48.
34. Hu, Z.; Tong, C. Synchronous fluorescence determination of DNA-based on the interaction between methylene blue and DNA. *Anal. Chim. Acta* **2007**, *587*, 187–193. [[CrossRef](#)]
35. Simonin, J.-P. On the comparison of pseudo-first order and pseudo-second order rate laws in the modeling of adsorption kinetics. *Chem. Eng. J.* **2016**, *300*, 254–263. [[CrossRef](#)]
36. Sheng, G.D.; Shao, D.D.; Ren, X.M.; Wang, X.Q.; Li, J.X.; Chen, Y.X.; Wang, X.K. Kinetics and thermodynamics of adsorption of ionizable aromatic compounds from aqueous solutions by as-prepared and oxidized multiwalled carbon nanotubes. *J. Hazard. Mater.* **2010**, *178*, 505–516. [[CrossRef](#)]
37. Wang, W.; He, R.; Yang, T.; Hu, Y.; Zhang, N.; Yang, C. Three-dimensional mesoporous calcium carbonate–silica frameworks thermally activated from porous fossil bryophyte: Adsorption studies for heavy metal uptake. *RSC Adv.* **2018**, *8*, 25754–25766. [[CrossRef](#)]
38. Dzhardimalieva, G.; Baimuratova, R.; Knerelman, E.; Davydova, G.; Kudaibergenov, S.; Kharissova, O.; Zhinzhiro, V.; Uflyand, I. Synthesis of Copper(II) Trimesinate Coordination Polymer and Its Use as a Sorbent for Organic Dyes and a Precursor for Nanostructured Material. *Polymers* **2020**, *12*, 1024. [[CrossRef](#)] [[PubMed](#)]
39. Mikhalyova, E.A.; Yakovenko, A.V.; Zeller, M.; Kiskin, M.A.; Kolomzarov, Y.V.; Eremenko, I.L.; Addison, A.W.; Pavlishchuk, V.V. Manifestation of  $\pi$ – $\pi$  Stacking Interactions in Luminescence Properties and Energy Transfer in Aromatically-Derived Tb, Eu and Gd Tris(pyrazolyl)borate Complexes. *Inorg. Chem.* **2015**, *54*, 3125–3133. [[CrossRef](#)] [[PubMed](#)]
40. Yang, Q.; Wang, Y.; Wang, J.; Liu, F.; Hu, N.; Pei, H.; Yang, W.; Li, Z.; Suo, Y.; Wang, J. High effective adsorption/removal of illegal food dyes from contaminated aqueous solution by Zr-MOFs (UiO-67). *Food Chem.* **2018**, *254*, 241–248. [[CrossRef](#)] [[PubMed](#)]
41. Wang, P.-L.; Xie, L.-H.; Joseph, E.A.; Li, J.-R.; Su, X.-O.; Zhou, H.-C. Metal-Organic Frameworks for Food Safety. *Chem. Rev.* **2019**, *119*, 10638–10690. [[CrossRef](#)]
42. Wood, R.; Foster, L.; Damant, A.; Key, P. *Analytical Methods for Food Additives*; CRC Press: Boca Raton, FL, USA, 2004.
43. McCune, L.M.; Kubota, C.; Stendell-Hollis, N.R.; Thomson, C.A. Cherries and Health: A Review. *Crit. Rev. Food Sci. Nutr.* **2010**, *51*, 1. [[CrossRef](#)]
44. Hanaa, A.-R.; Abdalsamad, K.M.E. Passivation characterization of nickel-based glassy alloys in artificial sea water. *Met. Mater. Int.* **2020**, *26*, 1688–1696.
45. Asgher, M.; Bhatti, H.N. Mechanistic and kinetic evaluation of biosorption of reactive azo dyes by free, immobilized and chemically treated Citrus sinensis waste biomass. *Ecol. Eng.* **2010**, *36*, 1660–1665. [[CrossRef](#)]
46. O'mahony, T.; Guibal, E.; Tobin, J. Reactive dye biosorption by Rhizopus arrhizus biomass. *Enzyme Microb. Technol.* **2002**, *31*, 456–463. [[CrossRef](#)]
47. Qin, Q.; Ma, J.; Liu, K. Adsorption of anionic dyes on ammonium-functionalized MCM-41. *J. Hazard. Mater.* **2009**, *162*, 133–139. [[CrossRef](#)]
48. Liu, H.; Gao, G.; Liu, J.; Bao, F.; Wei, Y.; Wang, H. Amide-functionalized ionic indium–organic frameworks for efficient separation of organic dyes based on diverse adsorption interactions. *CrystEngComm* **2019**, *21*, 2576–2584. [[CrossRef](#)]
49. Liu, J.; Zhang, X.-Y.; Hou, J.-X.; Liu, J.-M.; Jing, X.; Li, L.-J.; Du, J.-L. Functionalized Mn(II)-MOF based on host-guest interaction for selective and rapid capture of Congo red from water. *J. Solid State Chem.* **2019**, *270*, 697–704. [[CrossRef](#)]